Journal of Nuclear Medicine, published on March 13, 2020 as doi:10.2967/jnumed.119.227694

Title: Kinetic modeling and test-retest reproducibility of ^{11}C-EKAP and ^{11}C-FEKAP, novel agonist radiotracers for PET imaging of the kappa opioid receptor in humans

Authors: Mika Naganawa, Songye Li, Nabeel Nabulsi, Shu-fei Lin, David Labaree, Jim Ropchan, Hong Gao, Michael Mei, Shannan Henry, David Matuskey, Richard E. Carson, Yiyun Huang
Yale PET Center, Yale University, New Haven, CT, USA

Correspondence: Mika Naganawa,801 Howard Avenue,PO Box 208048,New Haven,CT,06520-8048,Phone:203-737-5582,Email:mika.naganawa@yale.edu

***Word Count*:** 5000

***Running Title*:** Kinetic analysis of novel kappa agonists

Acknowledgement: We appreciate the excellent technical assistance of the staff at the Yale University PET Center. This study was supported by research grants from the National Institute of Health (R21MH092664 & R33MH092664). No potential conflict of interest relevant to this article was reported. This publication was also made possible by CTSA Grant Number UL1 TR000142 from the National Center for Advancing Translational Sciences (NCATS), a component of the National Institutes of Health (NIH). The contents of this article are solely the responsibility of the authors and do not necessarily represent the official view of NIH.

ABSTRACT

The kappa opioid receptor (KOR) is implicated in various neuropsychiatric disorders. We previously evaluated an agonist tracer, ^{11}C-GR103545, for PET imaging of KOR in humans. Although ^{11}C-GR103545 showed high brain uptake, good binding specificity, and selectivity to KOR, it displayed slow kinetics and relatively large test-retest variability (TRV) of distribution volume (V_T) estimates (15%). Therefore we set out to develop two novel KOR agonist radiotracers, ^{11}C-EKAP and ^{11}C-FEKAP, and in nonhuman primates, both tracers exhibited faster kinetics and comparable binding parameters to ^{11}C-GR103545. The aim of this study was to assess their kinetic and binding properties in humans.

Methods: Six healthy subjects underwent 120-min test-retest PET scans with both ^{11}C-EKAP and ^{11}C-FEKAP. Metabolite-corrected arterial input functions were measured. Regional time-activity curves (TACs) were generated for 14 regions of interest. One- and two-tissue compartment (1TC, 2TC) models and the multilinear analysis-1 (MA1) method were applied to the regional TACs to calculate V_T. Time-stability of V_T values and test-retest reproducibility were evaluated. Levels of specific binding, as measured by the non-displaceable binding potential (BP_{ND}) for the three tracers (^{11}C-EKAP, ^{11}C-FEKAP and ^{11}C-GR103545), were compared using a graphical method.

Results: For both tracers, regional TACs were fitted well with the 2TC model and MA1 method (t^*=20min), but not with the 1TC model. Given the unreliably estimated parameters in several fits with the 2TC model and a good match between V_T values from MA1 and 2TC, MA1 was chosen as the appropriate model for both tracers. Mean MA1 V_T values were highest for ^{11}C-GR103545, followed by ^{11}C-EKAP, then ^{11}C-FEKAP. Minimum scan time for stable V_T measurement was 90 and 110 min for ^{11}C-EKAP and ^{11}C-FEKAP, respectively, compared with 140 min for ^{11}C-GR103545. The mean absolute TRV in MA1 V_T estimates was 7% and 18% for ^{11}C-EKAP and ^{11}C-FEKAP, respectively. BP_{ND} levels were similar for ^{11}C-FEKAP and ^{11}C-GR103545, but ~25% lower for ^{11}C-EKAP.

Conclusion: The two novel KOR agonist tracers showed faster tissue kinetics than ^{11}C-GR103545. Even with slightly lower BP_{ND}, ^{11}C-EKAP is judged to be a better tracer for imaging and quantification of KOR in humans, based on the shorter minimum scan time and excellent test-retest reproducibility of regional V_T valus.

KEYWORDS

Positron Emission Tomography, Kinetic modeling, Receptor imaging, Brain Imaging, Kappa Opioid Receptors

INTRODUCTION

The kappa opioid receptors (KOR) have been implicated in various psychiatric disorders including addictions, depression, and related mood disorders. We have previously developed and evaluated a set of KOR agonist and antagonist tracers, ^{11}C-GR103545 and ^{11}C-LY2795050, for imaging of the receptors in humans with positron emission tomography (PET) (*1,2*). The antagonist tracer, ^{11}C-LY2795050, proved to be suitable for imaging and quantifying KOR in the human brain (*3-5*). However, the agonist radiotracer, ^{11}C-GR103545, required a long scan time (140 min) for quantification of binding parameters due to its slow kinetics (*6*). In addition, the variability of outcome measures was higher than desirable (e.g.,15% on distribution volume (V_T) of test-retest study (*6*)). Therefore, KOR agonist tracers with faster kinetics and improved imaging properties are needed for reliable quantification of KOR configured in the high affinity state (*7*), to complement the antagonist tracer, which can be used to image and quantify the total KOR levels. We have developed two new agonist radiotracers, ^{11}C-EKAP (*8*) and ^{11}C-FEKAP (*9*) (Figure 1). Evaluation in non-human primates showed that they indeed have faster kinetics than ^{11}C-GR103545 with comparable binding specificity. In this paper, we report the first-in-human evaluation of ^{11}C-EKAP and ^{11}C-FEKAP to establish the appropriate kinetic models for analysis of imaging data, and to assess the test-retest reproducibility of binding parameters. The kinetic and binding properties of ^{11}C-EKAP and ^{11}C-FEKAP were also compared with those of ^{11}C-GR103545.

MATERIALS AND METHODS

Human Subjects

Six healthy subjects (20-51 years of age; 3 men and 3 women, body weight 75±13 kg) were enrolled in the study. PET imaging experiments were conducted under a protocol approved by the Yale University School of Medicine Human Investigation Committee and the Yale-New Haven Hospital Radiation Safety Committee, and in accordance with the United States federal guidelines and regulations for the protection of human research subjects contained in Title 45 Part 46 of the

Code of Federal Regulations (45 CFR 46). Written informed consent was obtained from all subjects. All subjects were healthy as assessed by a physical examination, comprehensive metabolic panel and complete blood count, and medical and psychiatric histories. Subjects had no current prescription or illicit drug use, no history of tobacco or nicotine use, no current uncontrolled medical conditions or history of neurological or psychiatric disorders. Females had negative pregnancy tests at intake and on the day of the scans. Magnetic resonance (MR) images were acquired on all subjects to verify no structural brain abnormalities and for PET image registration. MR imaging was performed on a 3T whole-body scanner (Trio,Siemens Medical Systems,Erlangen,Germany) with a circularly polarized head coil. The dimension and pixel size of MR images were 256×256×176 voxels and 0.98×0.98×1.0mm^3, respectively.

Radiotracer Synthesis

^{11}C-EKAP and ^{11}C-FEKAP were synthesized as previously described (*8,9*). Radiochemical purity of ^{11}C-EKAP and ^{11}C-FEKAP in the final product solution was >98%.

PET imaging Experiments

The subjects underwent two PET scans each with both ^{11}C-EKAP and ^{11}C-FEKAP. Per study plan, on the test study day, subjects underwent two PET scans each with both ^{11}C-EKAP and ^{11}C-FEKAP. Then, on the retest study day, each subject underwent two PET scans with both ^{11}C-EKAP and ^{11}C-FEKAP, in the scan order counterbalanced, except for one subject. One subject completed the retest scan 69 days after the test scan. Excluding this subject, the test and retest scans were 11±11 days apart for ^{11}C-EKAP and 10±8 days apart for ^{11}C-FEKAP. All PET scans were conducted on the High Resolution Research Tomograph (HRRT) (Siemens Medical Solutions,Knoxville,TN), which acquires 207 slices (1.2mm slice separation) with a reconstructed image resolution (FWHM) of ~3 mm. After a 6-min transmission scan for attenuation correction, PET scans were acquired for 120 min in list mode after intravenous administration of ^{11}C-EKAP or ^{11}C-FEKAP over 1 min by an automatic pump (Harvard PHD 22/2000, Harvard

Apparatus,Holliston,MA,USA). The injected mass limit was 0.02 μg/kg body weight. Dynamic scan data were reconstructed in 33 frames (6×0.5min, 3×1min, 2×2min, 22×5min) with corrections for attenuation, normalization, scatter, randoms, and deadtime using the MOLAR algorithm (*10*). Event-by-event motion correction (*11*) was included in the reconstruction based on measurements with the Polaris Vicra sensor (NDI Systems,Waterloo,Canada) with reflectors mounted on a swim cap worn by the subject.

Input Function Measurement

The radial artery was catheterized for blood sampling. Manual 0.5 mL samples were collected every 10 seconds for the first 90 seconds and thereafter twenty one samples (0.5 to 10 mL) were collected manually at selected time points. Plasma was obtained by centrifugation at 4°C (2,930*g* for 5min). Whole blood and plasma were counted in cross-calibrated gamma counters (1480&2480 WIZARD,PerkinElmer,Waltham,MA). In order to reduce noise in the data, the total plasma curve from ~5 min onward was fitted to a sum of exponentials.

Plasma Metabolite Analysis

Analysis of radioactive metabolites in the arterial plasma was performed using a modified automatic column-switching high performance liquid chromatography (HPLC) method(*12*). Plasma samples collected at 5, 15, 30, 60, and 90 min after injection were mixed with urea (8 M) and then filtered through 1.0 μm Whatman 13 mm GD/X syringe filters (GE,Florham Park,NJ,USA). Up to 5 mL of plasma filtrate was injected to the automatic column-switching HPLC system connecting a capture column (4.6×19mm) self-packed with Phenomenex Strata-X polymeric SPE sorbent and eluting with 1% MeCN in water at 2 mL/min for 4 min. The trapped activity in the capture column was then back flushed and eluted through a Phenomenex Luna C18 phenyl hexyl analytical column (4.6×250 mm,5 μm) with a mobile phase consisting of 45% MeCN and 55% 0.1 M ammonium formate (v/v) at a flow rate of 1.8 mL/min. HPLC eluate was fraction-collected and counted in the gamma counters. The fraction counts were corrected for volume and

decay. The unmetabolized parent fraction was calculated as the ratio of the sum of radioactivity in fractions containing the parent compound to the total amount of radioactivity collected, and fitted to an integrated gamma function (four fitted parameters: *a*, *b*, *c*, and *d*):

$$f(t) = a \times \left(1 - b \int_0^{ct} \exp(-u) u^{d-1} \mathrm{d}u \Big/ \int_0^{\infty} \exp(-u) u^{d-1} \mathrm{d}u \right) \quad (1)$$

In addition, the time-varying extraction efficiency of radioactivity in filtered plasma samples was determined, and normalized to that of reference plasma sample. The plasma input function was obtained as the product of the total plasma activity, the parent fraction, and the normalized extraction efficiency.

Measurement of Tracer Free Fraction in Plasma

Arterial blood samples were taken immediately before tracer injection for analysis of plasma free fraction (f_P). An ultrafiltration (Millipore Centrifree® micropartition device,4104,Billerica,MA,USA) method was used for measuring f_P of tracer in plasma in triplicate. The free fraction f_P was determined from the count ratio of ultrafiltrate to plasma.

Image Registration and Definition of Regions of Interest

Regions of interest (ROI) were defined in the Automated Anatomical Labeling (AAL) for SPM2 (*13*) in Montreal Neurological Institute (MNI) space (*14*). After hardware motion correction, the dynamic PET images were co-registered to the early summed PET images from 0 to 10 min post-injection using a 6-parameter mutual information algorithm (*15*) (FLIRT, FSL) to eliminate any residual motion. The summed PET image was then co-registered to the individual subject's T1-weighted 3T MR image (6-parameter rigid registration) and then co-registered to the AAL template in MNI space using a nonlinear transformation (Bioimage suite) (*16*). Using the combined transformations from template to individual subject's PET space, regional time-activity curves (TACs) were generated for 14 ROIs: amygdala, caudate, centrum semiovale, cerebellum, anterior

cingulate cortex, frontal cortex, globus pallidus, hippocampus, insula, occipital cortex, posterior cingulate cortex, putamen, temporal cortex, and thalamus.

Quantitative Analysis

The outcome measures were derived with kinetic analysis of the regional TACs using the arterial plasma input function. The distribution volume (V_T)(*17*) was calculated using one- and two-tissue compartment (1TC, 2TC) models and the multilinear analysis-1 (MA1) method (*18*). The test scans (n=6) were used for kinetic model assessment. The time-stability of V_T estimates was assessed by comparing V_T values from shortened scans, ranging from 110 to 50 min, to the 120-min V_T value using the MA1 (t^*=20 min) model. The ratio of V_T values from the shortened scan to that from the 120-min scan was computed for each ROI and duration. The following two criteria were adopted to determine a minimum scan duration (*19*): a) the average of the ratio was between 0.95 and 1.05; b) the inter-individual standard deviation of the ratio was <0.1. All modeling was performed with in-house programs written with IDL 8.0 (ITT Visual Information Solutions,Boulder,CO,USA). For parameter estimation, data points were weighted based on noise equivalent counts in each frame. Percentage standard error (%SE) was estimated from the theoretical parameter covariance matrix. %SE was used to examine the reliability of individual fits (fits were considered unreliable when %SE of V_T>10%).

As KOR is distributed throughout the brain, no reference region was available. To predict which KOR radiotracer will show higher specific binding signals, the graphical method of Guo et al. (Guo plot)(*20*) was applied to compare ^{11}C-EKAP and ^{11}C-FEKAP with ^{11}C-GR103545. The equation for the Guo plot to compare tracer A and tracer B is described as the following:

$$\mathbf{V}_{\mathrm{T}}^{\mathrm{B}} = \frac{f_{\mathrm{P}}^{\mathrm{B}}}{f_{\mathrm{P}}^{\mathrm{A}}}\frac{K_{\mathrm{D}}^{\mathrm{A}}}{K_{\mathrm{D}}^{\mathrm{B}}}\mathbf{V}_{\mathrm{T}}^{\mathrm{A}} + V_{\mathrm{ND}}^{\mathrm{B}}\left(1 - \frac{BP_{\mathrm{ND}}^{\mathrm{B}}}{BP_{\mathrm{ND}}^{\mathrm{A}}}\right)$$

When plotting $\mathbf{V}_T^B$ (y-axis) against $\mathbf{V}_T^A$ (x-axis), the sign of y-intercept predicts which tracer will produce a bigger BP_{ND}. The mean V_T values across test scans for ^{11}C-EKAP and ^{11}C-FEKAP and

the mean V_T values from previous study (*6*) for ^{11}C-GR103545 were used for the Guo plot. The regression line was estimated with total least squares method with weights that are proportional to the inverse of inter-subject standard deviation (SD). The relative BP_{ND} values can be estimated from the measured intercept if V_{ND} of tracer B is known.

For the test-retest data, results were evaluated according to three criteria: relative test-retest variability (TRV), absolute test-retest variability (aTRV), and intra-class correlation coefficient (ICC). The test and retest scan >1 month apart (n=1) was excluded. TRV was calculated as the difference between the parameters in the test and retest scans divided by their average. The mean of TRV denotes the presence of a trend between the two scans, and the standard deviation of TRV is an index of the variability in the difference of two estimates. aTRV is the absolute value of TRV and comparable to the error in a single measurement.

RESULTS

Injection Parameters and Plasma Analysis

The mean and standard deviation of the administered mass of ^{11}C-EKAP and ^{11}C-FEKAP was 1.18±0.32μg (range,0.80–1.65μg) and 1.12±0.35μg (range,0.62–1.61μg), respectively. The mean administered activity of ^{11}C-EKAP and ^{11}C-FEKAP was 580±111MBq (range,382–746 MBq) and 483±197MBq (range, 152–730MBq), respectively. There were no adverse or clinically detectable pharmacologic effects in any of the 6 subjects. No significant changes in vital signs or the results of laboratory studies were observed.

Table 1 lists the injected radioactivity dose, molar activity at the time of injection, injected mass, and plasma free fractions. There were no significant differences between test and retest scans with both tracers in the injected dose, nor in the injected mass, or plasma free fraction. Figure 2 displays the parent fractions and metabolite-corrected plasma curves from test-retest study for both tracers. The parent fractions were similar between the test and retest scans for both tracers. ^{11}C-FEKAP displayed a lower parent fraction than ^{11}C-EKAP in plasma. The mean parent fractions at

60-min post-injection were 32%±7% and 34%±6% for the test and retest scans with ^{11}C-EKAP and 23%±5% and 21%±5% for the test and retest scans with ^{11}C-FEKAP. However, the actual parent radioactivity levels of the two tracers were quite similar (Figures 2C and D), suggesting that the difference in parent fraction was due to different clearance rates of the radiolabeled metabolies. The f_P was 0.25±0.03% for ^{11}C-EKAP (n=12) and 0.06±0.01% for ^{11}C-FEKAP (n=12).

Modeling Results

Radioactivity distribution in the brain was heterogeneous, and the distribution pattern was similar between ^{11}C-EKAP and ^{11}C-FEKAP (Figure 3). Regional TACs for representative brain regions are shown in Figure 3. The TACs reached peak at ~20 and ~40 min post-injection of ^{11}C-EKAP and ^{11}C-FEKAP, respectively (Figure 4). Typical examples of curve fittings with 1TC and 2TC models and MA1 are also shown in Figure 4. Regional TACs were fitted well with the 2TC and MA1 models, and to a lesser extent with the 1TC model. The parameters of 2TC model were not reliably estimated (%SE>10% in V_T) in a few cases, especially in the amygdala. Given the low ICC value of MA1 V_T for ^{11}C-EKAP in the amygdala, quantification was still difficult in the amygdala even with MA1, due to the combination of small ROI size and slow kinetics. Mean K_1 values (mL/cm^3/min) in the 1TC model ranged from 0.09 (centrum semiovale) to 0.21 (putamen) for ^{11}C-EKAP and from 0.033 (centrum semiovale) to 0.076 (insula) for ^{11}C-FEKAP. There were excellent correlations in V_T values between the kinetic models (^{11}C-EKAP:$V_{T(1TC)}$=0.96×$V_{T(2TC)}$-0.53,R^2=0.98, and $V_{T(MA1,t^*=20min)}$=1.02×$V_{T(2TC)}$-0.28,R^2=0.98; ^{11}C-FEKAP:$V_{T(1TC)}$=0.92×$V_{T(2TC)}$-0.17,R^2=0.98, and $V_{T(MA1,t^*=20min)}$=1.02×$V_{T(2TC)}$+0.11,R^2=1.00). These comparisons were performed for the regions with good identifiability, i.e.,%SE of V_T<10% with the 2TC model. For both tracers, t^* for MA1 was selected as 20 min by comparing the MA1 V_T values with 2TC V_T values. Based on the good and consistent quality of fit and comparison with 2TC V_T values, the MA1 model was chosen for both tracers.

Regional V_T values estimated using 1TC, 2TC, and MA1 (t^*=20 min) and the minimum scan time for the MA1 model are summarized in Table 2. For both ^{11}C-EKAP and ^{11}C-FEKAP, high V_T values were seen in the amygdala, insula, and anterior cingulate cortex, and lower values were in the centrum semiovale, cerebellum, and thalamus. The intersubject V_T variability was higher for ^{11}C-FEKAP (MA1:23-39%) than ^{11}C-EKAP (MA1:14-26%). The minimum scan durations to obtain stable V_T values were 90 and 110 min for ^{11}C-EKAP and ^{11}C-FEKAP, respectively.

Test-retest Reproducibility

The aTRV of MA1 V_T estimates was good (4-8%) for ^{11}C-EKAP across all regions except for the amygdala (17%) (Table 3). The aTRV of ^{11}C-FEKAP V_T was higher in all regions (13-26%) than those of ^{11}C-EKAP. Test-retest reproducibility of V_T measured by ICC was excellent (0.78-0.98) for ^{11}C-EKAP in all regions except for the amygdala (0.19). ICC of ^{11}C-FEKAP was also generally good (0.63-0.83) except for three regions: anterior cingulate cortex (0.57), cerebellum (0.47), and thalamus (0.55).

Comparison of ^{11}C-EKAP and ^{11}C-FEKAP with ^{11}C-GR103545

Figure 5 shows the Guo plots to compare the regional V_T values of ^{11}C-EKAP, ^{11}C-FEKAP, and ^{11}C-GR103545. An excellent linear relationship was observed between the V_T values across regions, which suggests that the tracers bind to the same target with the same distribution. Based on the of y-intercepts in Figure 5, ^{11}C-GR103545 has the highest binding potential, followed by ^{11}C-FEKAP, and the lowest for ^{11}C-EKAP. The regression yielded a negative y-intercept vs. ^{11}C-GR103545 (^{11}C-EKAP,-2.41;^{11}C-FEKAP,-0.97). Using the mean population non-displaceable distribution volume of ^{11}C-GR103545 (V_{ND},3.4 mL/cm^3) and a range of BP_{ND} values (1.1-7.4) of ^{11}C-GR103545 taken from the literature, regional BP_{ND} values were estimated to range from 0.6 to 4.3 for ^{11}C-EKAP and from 0.8 to 5.7 for ^{11}C-FEKAP. The ratio of BP_{ND}(^{11}C-EKAP)/BP_{ND}(^{11}C-FEKAP) was 0.75.

DISCUSSION

We evaluated the kinetics of two novel kappa opioid receptor agonists, ^{11}C-EKAP and ^{11}C-FEKAP as PET radiotracers in humans, in comparison with ^{11}C-GR103545, an agonist tracer previously reported by us (*6*).

Three kinetic models were compared for ^{11}C-EKAP and ^{11}C-FEKAP with arterial input functions. Regional TACs were fitted well by the 2TC model and MA1 for both tracers. The V_T values were close to identical between the 2TC model and MA1. As seen for ^{11}C-GR103545 (*6*), the 2TC model produced V_T estimates with large errors in some fits, especially in the amygdala. On the other hand, the MA1 method estimated V_T reliably in all fits and produced similar V_T values for t^* setting from 10 to 30 min. For both tracers, MA1 is the model of choice. For the same reason, MA1 (t^*=40 min) was also selected for ^{11}C-GR103545.

The rank order of V_T and tracer uptake pattern were the same between ^{11}C-EKAP, ^{11}C-FEKAP, and ^{11}C-GR103545. As seen with ^{11}C-GR103545, the thalamus had the lowest V_T value for both ^{11}C-EKAP and ^{11}C-FEKAP. For the 1TC K_1 (mL/cm^3/min) values, ^{11}C-EKAP showed the highest K_1 values (0.09-0.21), followed by ^{11}C-GR103545 (0.06-0.14) and ^{11}C-FEKAP (0.033-0.076). For the MA1 V_T (mL/cm^3) values, ^{11}C-GR103545 (7.3-26.9) gave the highest V_T values, followed by ^{11}C-EKAP (5.4-21.6) and ^{11}C-FEKAP (2.3-9.6).

The average test-retest variability (aTRV) of V_T values was found to be 7% (range:4-17%) for ^{11}C-EKAP, 18% (range:13-26%) for ^{11}C-FEKAP, and 15% (range:8-41%) for ^{11}C-GR103545. Minimum scan time required for stable V_T estimates was 90, 110, and 140 min, respectively, for ^{11}C-EKAP, ^{11}C-FEKAP, and ^{11}C-GR103545. Since these tracers are carbon-11 labeled, a short scan time (e.g.,≤90 min) is preferred. ^{11}C-FEKAP, with aTRV>15% in most regions, may not be useful for evaluating group differences in receptor availability.

Even though ^{11}C-EKAP showed a better reproducibility than the other two tracers, the small number of subjects (n=5) requires a careful interpretation of the test-retest results and numerical values of TRV, aTRV, and ICC. TRV (aTRV=TRV for n=1) for the excluded subject

(scanned 69 days apart) was 33±3% for ^{11}C-EKAP and 16±5% for ^{11}C-FEKAP (across regions). This indicates that long term variability of kappa expression might be larger than the test-retest variability reported here. However, more data are required to verify this result.

Since the KOR is ubiquitously distributed throughout the brain, there are no appropriate reference regions in humans for use in kinetic modeing. This has been demonstrated in the studies of other KOR agonist and antagonist radiotracers (*3,6*). Therefore, we used the Guo plot to compare the magnitude of non-displaceable binding potential (BP_{ND}) between the two new agonist radiotracers. The linearity of the Guo plot indicates whether the tracers bind with the same target. An almost perfect linear relation was observed between ^{11}C-EKAP and ^{11}C-FEKAP V_T values (Figure 5C), but the linearity between ^{11}C-EKAP or ^{11}C-FEKAP and ^{11}C-GR103545 was not as good (Figure 5A and 5B). This does not necessarily mean that ^{11}C-GR103545 binds with a target different from the two new tracers, as the results for ^{11}C-EKAP and ^{11}C-FEKAP are from the same group of subjects who received both tracers (while those for ^{11}C-GR103545 are not). As there are several regions (e.g.,amygdala) with high intra-subject V_T variability, weighting is required to compute the regression line of the Guo plot. We used the inverse of the inter-subject SD of V_T values as weighting and the total least squares method to take the inter-subject SD of V_T values for both tracers into account. The *y*-intercept of the Guo plot consists of V_{ND} and a ratio of BP_{ND} values between the two tracers. By substituting the population V_{ND} value (3.4 mL/cm^3) and a range of BP_{ND} values (1.1-7.4) from ^{11}C-GR103545 into the *y*-intercept, the BP_{ND} values of ^{11}C-EKAP and ^{11}C-FEKAP can be calculated: The relative binding potentials are 1.71 (BP_{ND}(^{11}C-GR103545)/BP_{ND}(^{11}C-EKAP)) and 1.28 (BP_{ND}(^{11}C-GR103545)/BP_{ND}(^{11}C-FEKAP)). ^{11}C-FEKAP BP_{ND} values are similar to those of ^{11}C-GR103545 BP_{ND}, while ^{11}C-EKAP BP_{ND} values are lower. Thus, the specific binding of ^{11}C-EKAP is predicted to be ~25% lower than that of ^{11}C-FEKAP. The *in vivo* affinity ratio can be derived from the slope of Guo plot and the f_P values (K_D(^{11}C-EKAP)/K_D(^{11}C-FEKAP)≈2). The order of *in vitro* affinities is inverted (K_D(^{11}C-EKAP)/K_D(^{11}C-FEKAP)=0.7 (*8,9*)). However, for both *in vitro* and *in vivo* studies, a K_D ratio of 2 is unlikely to be

significantly different from identity, and it is not uncommon that disparities in *in vivo* and *in vitro* affinity measurements are found, due to multiple factors such as measurement temperature, cell/receptor types, and experimental procedures used *in vitro*.

In summary, the two novel KOR agonist radiotracers ^{11}C-EKAP and ^{11}C-FEKAP display faster kinetic properties than ^{11}C-GR103545. ^{11}C-EKAP displays much better test-retest reproducibility and requires a shorter scan time to obtain stable V_T estimates. Although ^{11}C-EKAP is predicted to have ~25% lower BP_{ND} values than ^{11}C-FEKAP, the range of BP_{ND} values for ^{11}C-EKAP is very useful (~1-4). Therefore, ^{11}C-EKAP is judged to be a better tracer than ^{11}C-FEKAP for the imaging and quantification of KOR agonist binding in humans.

Disclosure/Conflict of interest

The authors declare no conflict of interest.

KEY POINTS

QUESTION: Which agonist radiotracer shows suitable kinetic property to quantify kappa opioid receptor (KOR) in the human brain, ^{11}C-EKAP or ^{11}C-FEKAP?

PERTINENT FINDINGS: The two novel KOR agonist tracers show faster tissue kinetics than the current tracer ^{11}C-GR103545. ^{11}C-EKAP is deemed to be a better tracer for imaging and quantification of KOR, based on the shorter minimum scan time and excellent test-retest reproducibility.

IMPLICATIONS FOR PATIENT CARE: ^{11}C-EKAP shortens the scan time from 140 min to 90 min.

REFERENCES

1. Zheng MQ, Nabulsi N, Kim SJ, et al. Synthesis and evaluation of ^{11}C-LY2795050 as a kappa-opioid receptor antagonist radiotracer for pet imaging. *J Nucl Med.* 2013;54:455-463.
2. Ravert HT, Mathews WB, Musachio JL, Scheffel U, Finley P, Dannals RF. [^{11}C]-methyl 4-[(3,4-dichlorophenyl)acetyl]-3-[(1-pyrrolidinyl)-methyl]-1- piperazinecarboxylate ([^{11}C]GR89696): Synthesis and in vivo binding to kappa opiate receptors. *Nucl Med Biol.* 1999;26:737-741.
3. Naganawa M, Zheng MQ, Nabulsi N, et al. Kinetic modeling of (11)C-LY2795050, a novel antagonist radiotracer for pet imaging of the kappa opioid receptor in humans. *J Cereb Blood Flow Metab.* 2014;34:1818-1825.
4. Naganawa M, Zheng MQ, Henry S, et al. Test-retest reproducibility of binding parameters in humans with 11C-LY2795050, an antagonist pet radiotracer for the kappa opioid receptor. *J Nucl Med.* 2015;56:243-248.
5. Naganawa M, Dickinson GL, Zheng MQ, et al. Receptor occupancy of the kappa-opioid antagonist LY2456302 measured with positron emission tomography and the novel radiotracer 11C-LY2795050. *J Pharmacol Exp Ther.* 2016;356:260-266.
6. Naganawa M, Jacobsen LK, Zheng MQ, et al. Evaluation of the agonist pet radioligand [(1)(1)C]GR103545 to image kappa opioid receptor in humans: Kinetic model selection, test-retest reproducibility and receptor occupancy by the antagonist pf-04455242. *Neuroimage.* 2014;99:69-79.
7. Shalgunov V, van Waarde A, Booij J, Michel MC, Dierckx R, Elsinga PH. Hunting for the high-affinity state of G-protein-coupled receptors with agonist tracers: Theoretical and practical considerations for positron emission tomography imaging. *Med Res Rev.* 2018;39:1014-1052.
8. Li S, Zheng MQ, Naganawa M, et al. Development and in vivo evaluation of a kappa-opioid receptor agonist as a pet radiotracer with superior imaging characteristics. *J Nucl Med.* 2019;60:1023-1030.
9. Li S, Zheng MQ, Naganawa M, et al. Novel kappa opioid receptor agonist as improved pet radiotracer: Development and in vivo evaluation. *Mol Pharm.* 2019;16:1523-1531.
10. Carson RE, Barker WC, Liow JS, Johnson CA. Design of a motion-compensation OSEM list-mode algorithm for resolution-recovery reconstruction for the hrrt. *IEEE 2003 Nuclear Science Symposium Conference Record.* 2003;5:3281-3285.
11. Jin X, Chan C, Mulnix T, et al. List-mode reconstruction for the Biograph mCT with physics modeling and event-by-event motion correction. *Phys Med Biol.* 2013;58:5567-5591.
12. Hilton J, Yokoi F, Dannals RF, Ravert HT, Szabo Z, Wong DF. Column-switching HPLC for the analysis of plasma in pet imaging studies. *Nucl Med Biol.* 2000;27:627-630.
13. Tzourio-Mazoyer N, Landeau B, Papathanassiou D, et al. Automated anatomical labeling of activations in SPM using a macroscopic anatomical parcellation of the MNI MRI single-subject brain. *Neuroimage.* 2002;15:273-289.
14. Holmes CJ, Hoge R, Collins L, Woods R, Toga AW, Evans AC. Enhancement of MR images using registration for signal averaging. *J Comput Assist Tomogr.* 1998;22:324-333.
15. Viola P, Wells WM. Alignment by maximization of mutual information. *Int J Comput Vision.* 1997;24:137-154.
16. Papademetris X, Jackowski M, Rajeevan N, Constable RT, Staib LH. Bioimage suite: An integrated medical image analysis suite. *Insight J.* 2005.

17. Innis RB, Cunningham VJ, Delforge J, et al. Consensus nomenclature for in vivo imaging of reversibly binding radioligands. *J Cereb Blood Flow Metab.* 2007;27:1533-1539.

18. Ichise M, Toyama H, Innis RB, Carson RE. Strategies to improve neuroreceptor parameter estimation by linear regression analysis. *J Cereb Blood Flow Metab.* 2002;22:1271-1281.

19. Frankle WG, Huang Y, Hwang DR, et al. Comparative evaluation of serotonin transporter radioligands ^{11}C-DASB and ^{11}C-McN 5652 in healthy humans. *J Nucl Med.* 2004;45:682-694.

20. Guo Q, Owen DR, Rabiner EA, Turkheimer FE, Gunn RN. A graphical method to compare the in vivo binding potential of pet radioligands in the absence of a reference region: Application to [(1)(1)C]PBR28 and [(1)(8)F]PBR111 for tspo imaging. *J Cereb Blood Flow Metab.* 2014;34:1162-1168.

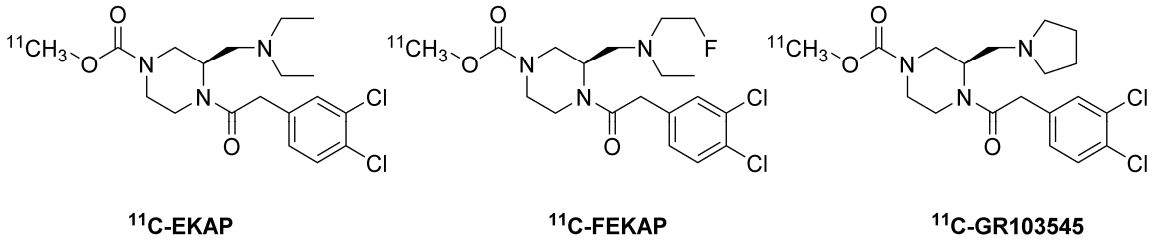

Figure 1: Molecular structures of C-EKAP, ^{11}C-FEKAP, and ^{11}C-GR104545.

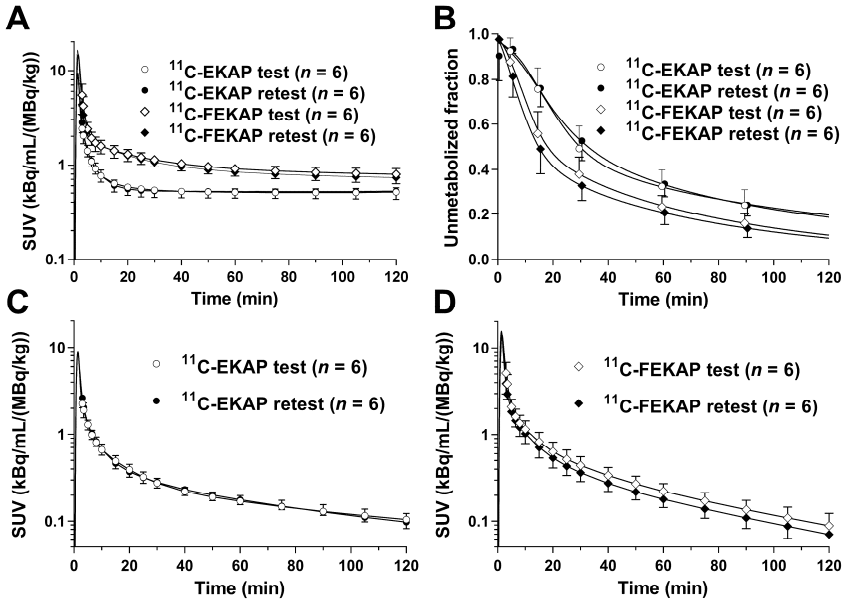

Figure 2: Mean±SD of total plasma activity (A), parent fraction in the plasma (B), and metabolite-corrected plasma activity over time for ^{11}C-EKAP (C) and ^{11}C-FEKAP (D). Panels A, C and D are displayed in SUV units [concentration/(injected dose/body weight)].

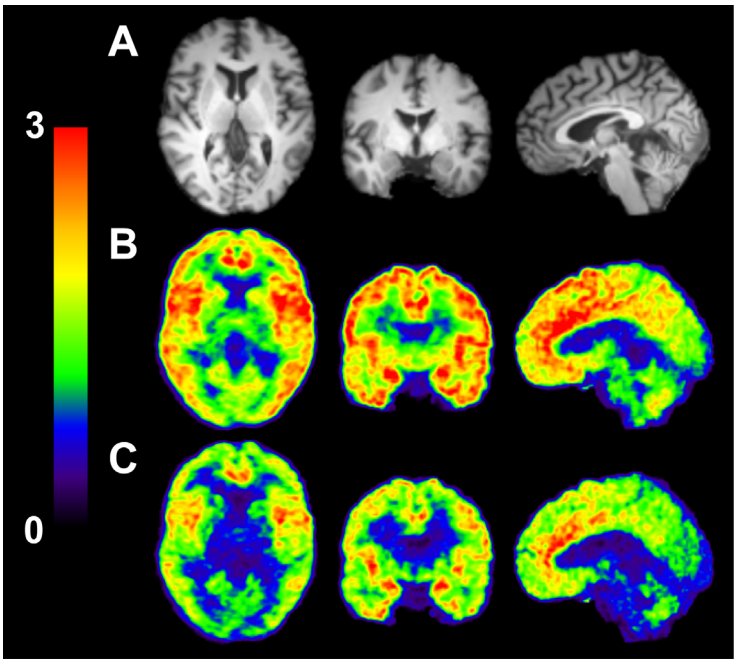

Figure 3: Typical MR (A) and co-registered PET images summed from 30 to 90 min after tracer injection for ^{11}C-EKAP (B) and ^{11}C-FEKAP (C). Activity is expressed as SUV [concentration/(injected dose/body weight)].

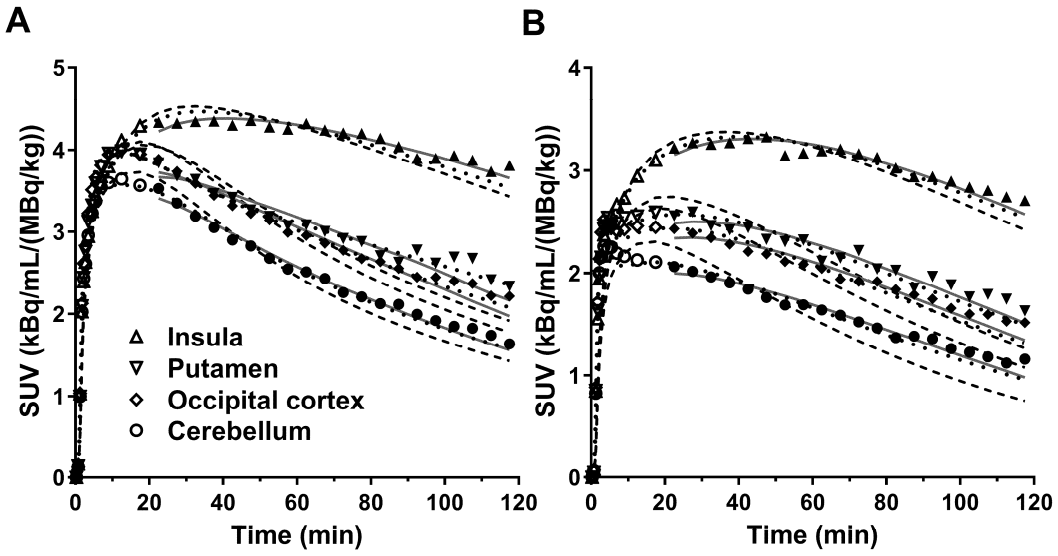

Figure 4: Time-activity curves in four ROIs for ^{11}C-EKAP (A) and ^{11}C-FEKAP (B) with the 1TC (break), 2TC (dotted), and MA1 (t^*=20 min, solid) fits. For each region, the symbols correspond to the measured regional activity.

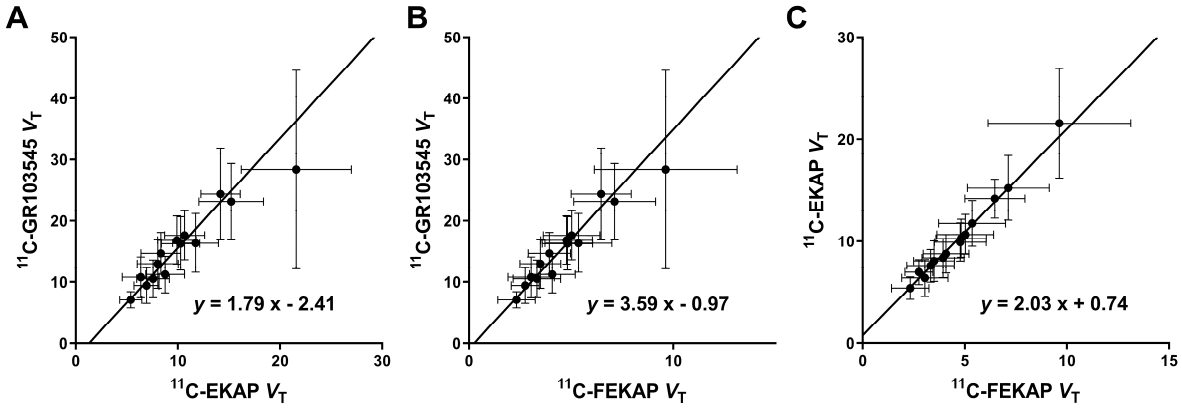

Figure 5: Comparison of V_T values of ^{11}C-EKAP, ^{11}C-FEKAP, and ^{11}C-GR103545. Error bars show the inter-subject variability (standard deviation).

Table 1: Subject Information and PET Scan Parameters

	Test-retest (^{11}C-EKAP)			Test-retest (^{11}C-FEKAP)		
	Test (*n*=6)	Retest (*n*=6)	*P*-value	Test (*n*=6)	Retest (*n*=6)	*P*-value
Injected dose (MBq)	625±85	534±121	0.07	447±180	519±223	0.38
Molar activity at time of injection (MBq/nmol)	244±63	205±84	0.35	188±119	237±126	0.43
Injected mass (µg)*	1.15±0.31	1.20±0.35	0.71	1.21±0.39	1.03±0.32	0.34
Plasma free fraction	24.6±2.8%	24.5±3.1%	0.96	6.3±0.9%	6.2±0.8%	0.73

*Mass limit 0.02 µg/kg.

Table 2: Regional distribution volumes in test scans

Regions	Regional distribution volume (mL/cm^3)						Minimum scan duration (min)	
	^{11}C-EKAP (*n*=6)			^{11}C-FEKAP (*n*=6)			^{11}C-EKAP (*n*=6)	^{11}C-FEKAP (*n*=6)
	1TC (%COV)	2TC (%COV)	MA1 (%COV)	1TC (%COV)	2TC (%COV)	MA1 (%COV)	MA1	MA1
Amygdala	19.9(22%)	†18.1(6%)	21.6(25%)	9.1(33%)	*9.0(39%)	9.6(36%)	90	90
Insula	13.9(21%)	14.7(19%)	15.2(21%)	6.4(27%)	‡6.8(31%)	7.1(28%)	80	70
Ant. cingulate cortex	13.1(13%)	13.8(13%)	14.2(14%)	5.8(21%)	6.2(22%)	6.5(23%)	70	70
Globus pallidus	10.7(19%)	11.5(18%)	11.7(19%)	4.6(28%)	5.3(29%)	5.4(30%)	70	60
Temporal cortex	9.8(18%)	11.0(21%)	10.7(18%)	4.3(25%)	4.8(27%)	5.0(28%)	80	90
Putamen	9.3(18%)	10.8(21%)	10.3(18%)	3.9(23%)	4.6(26%)	4.8(26%)	80	100
Frontal cortex	9.0(19%)	10.3(23%)	9.9(19%)	4.1(25%)	4.6(27%)	4.8(27%)	80	90
Hippocampus	7.6(21%)	9.1(26%)	8.8(22%)	3.2(23%)	3.8(27%)	4.1(27%)	80	90
Occipital cortex	7.5(20%)	8.7(21%)	8.3(19%)	3.2(26%)	3.8(29%)	3.9(30%)	80	90
Caudate	7.5(24%)	8.1(26%)	8.0(24%)	2.9(27%)	3.4(29%)	3.5(30%)	50	80
Post. cingulate cortex	6.8(27%)	‡7.2(25%)	7.6(26%)	2.7(29%)	3.1(30%)	3.3(30%)	80	100
Cerebellum	5.7(32%)	6.6(29%)	6.4(29%)	2.1(34%)	‡2.6(32%)	3.0(37%)	80	100
Thalamus	4.8(20%)	‡5.2(15%)	5.4(20%)	1.5(22%)	‡1.9(20%)	2.3(39%)	80	110

%COV is variability across subjects. Relative standard error > 10% was excluded: † *n*=4, ‡ *n*=5, * *n*=2

Table 3: Test-retest variability and reproducibility of distribution volume

Regions	^{11}C-EKAP(n=5)			^{11}C-FEKAP(n=5)		
	aTRV(%)	TRV(%)	ICC	aTRV(%)	TRV(%)	ICC
Amygdala	17±14	4±23	0.19	24±11	-12±26	0.72
Insula	7±6	1±10	0.85	19±9	-5±23	0.63
Ant. cingulate cortex	7±5	3±9	0.78	17±6	-2±20	0.57
Globus pallidus	8±4	2±10	0.82	16±5	-4±18	0.83
Temporal cortex	6±5	0±8	0.91	17±5	-1±20	0.68
Putamen	6±6	-3±9	0.86	13±5	-2±16	0.79
Frontal cortex	5±6	-1±8	0.91	16±5	-3±19	0.71
Hippocampus	5±5	-1±8	0.92	17±7	-5±19	0.72
Occipital cortex	4±5	-1±6	0.96	17±5	-2±19	0.73
Caudate	6±7	-3±9	0.95	17±5	-3±19	0.78
Post. cingulate cortex	7±6	-1±10	0.95	18±8	-3±21	0.74
Cerebellum	6±5	0±8	0.98	26±14	0±32	0.47
Thalamus	5±7	-2±8	0.87	20±14	3±26	0.55